# SMALL DIAMETER WAVEGUIDE FOR WIDEBAND ACOUSTIC EMISSION

**M. A. HAMSTAD**
National Institute of Standards and Technology, Materials Reliability Division (853), 325 Broadway, Boulder, CO 80305-3328 and University of Denver, School of Engineering and Computer Science, Department of Engineering, Denver, CO 80208.

## Abstract

The signals obtained from two wideband conical sensors were compared in the time, frequency and time/frequency domains. The signals were generated by pencil-lead breaks on the surface (out-of-plane) or close to the midplane of the edge (in-plane) of a large (1220 mm by 1525 mm) aluminum alloy plate (thickness of 3.1 mm). One sensor was coupled to the plate surface by vacuum grease at a propagation distance of 254 mm, and the other sensor was coupled with vacuum grease to the end of a nominal 300 mm or 400 mm long small-diameter waveguide. The other end of the waveguide was coupled to the plate surface by vacuum grease at a 254-mm propagation distance. The waveguides were either aluminum alloy (1.59-mm or 3.18-mm diameter) or brass (1.59-mm diameter). The goal was to determine how closely the waveguide sensor signal duplicated the signal obtained from the plate-mounted sensor. Results were considered in the light of group velocity diagrams for the aluminum plate and the aluminum rods. The sensor mounted on the 1.59-mm diameter aluminum waveguide provided a signal that closely duplicated the signal from the plate-mounted sensor.

**Keywords:** Acoustic emission, waveguides, wideband sensors

## Introduction

Waveguides are used in acoustic emission (AE) technology in several situations. Some of these are (i) a test sample at an elevated temperature above the maximum operating temperature of the AE sensor; (ii) a test item covered with insulation such that typical sensor mounting is inconvenient or precluded; and (iii) a test specimen that is either very small or sufficiently irregular that it does not allow mounting a sensor directly on the specimen. A recent publication [1] referenced several waveguide studies, and it studied waveguides for AE applications. This study did not include wideband small-aperture sensors nearly flat with frequency.

The purpose of the research reported here was to examine whether the combination of a wideband conical-type AE sensor with a waveguide of small diameter would result in the waveguide-mounted sensor signal closely duplicating the signal from a specimen-mounted sensor of the same design.

---

This paper is a contribution of the U.S. National Institute of Standards and Technology and not subject to copyright in the United States. Trade and company names are included only for complete scientific/technical description; endorsement is neither intended nor implied.

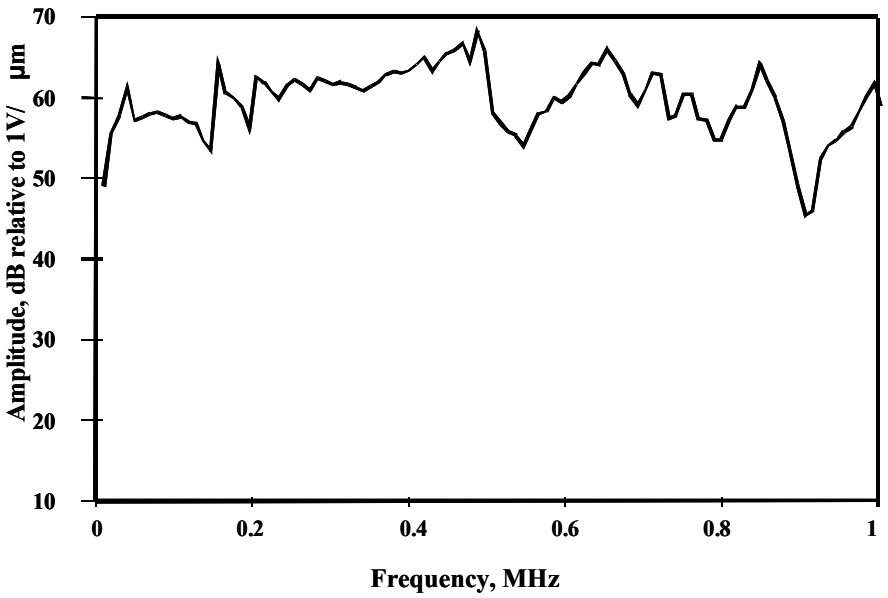


Fig. 1 NIST-based calibration of conical sensor at the preamplifier calibration gain (about 10 dB); out-of-plane displacement response.

## Experiment

The conical sensors used in the research were manufactured at the National Institute of Standards and Technology (NIST) in Boulder, Colorado. This sensor design was fully described in two previous publications [2, 3]. Figure 1 shows the out-of-plane displacement-based frequency response of a sensor with this design when it was calibrated with its associated preamplifier at its "calibration" gain of about 10 dB (according to the manufacturer [4]). The results in this figure were generated at NIST in Gaithersburg, Maryland.

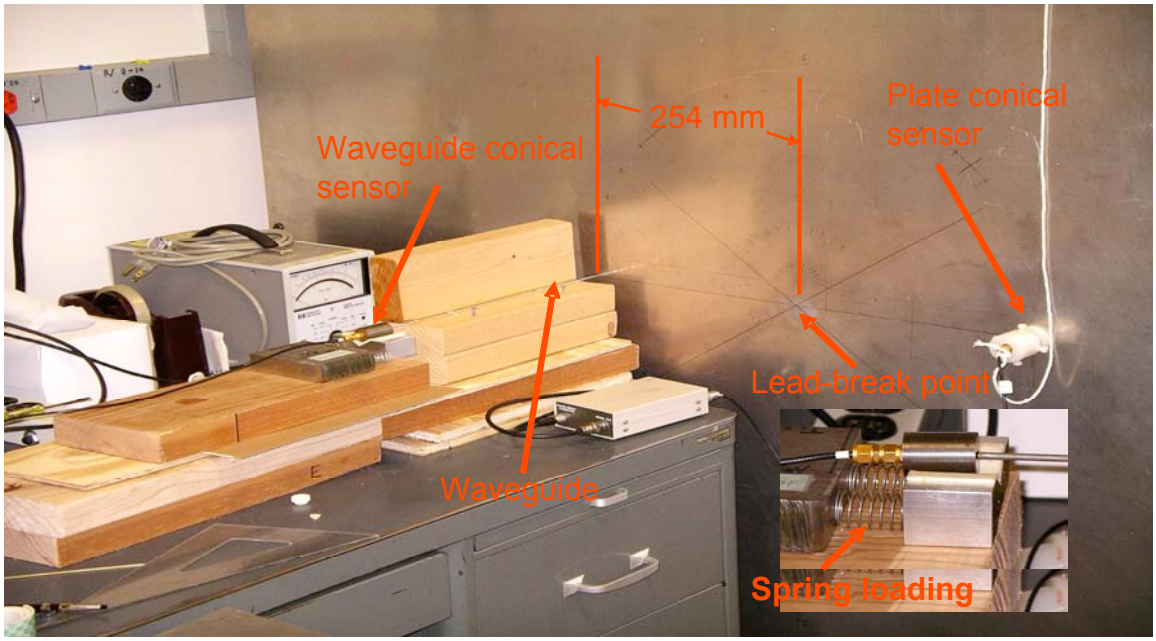


Fig. 2 Photograph of test setup for out-of-plane pencil-lead-break source with an insert of spring loading.

The sensor, which features a conical piezoelectric element with a 1.5-mm aperture, has internal electronics that are compatible with the preamplifier manufactured in Japan [4]. The internal electronics increase the sensitivity beyond that typical of a wideband sensor. In the experiments reported here, two such sensors were used. Each sensor was connected to a preamplifier using the "calibration" gain. Beyond the preamplifier, the signal was filtered by a high-pass, 50 kHz, four-pole Butterworth passive filter. The signal from the filter was recorded by a 12-bit digital recorder at a sample rate of 0.1 μs per point.

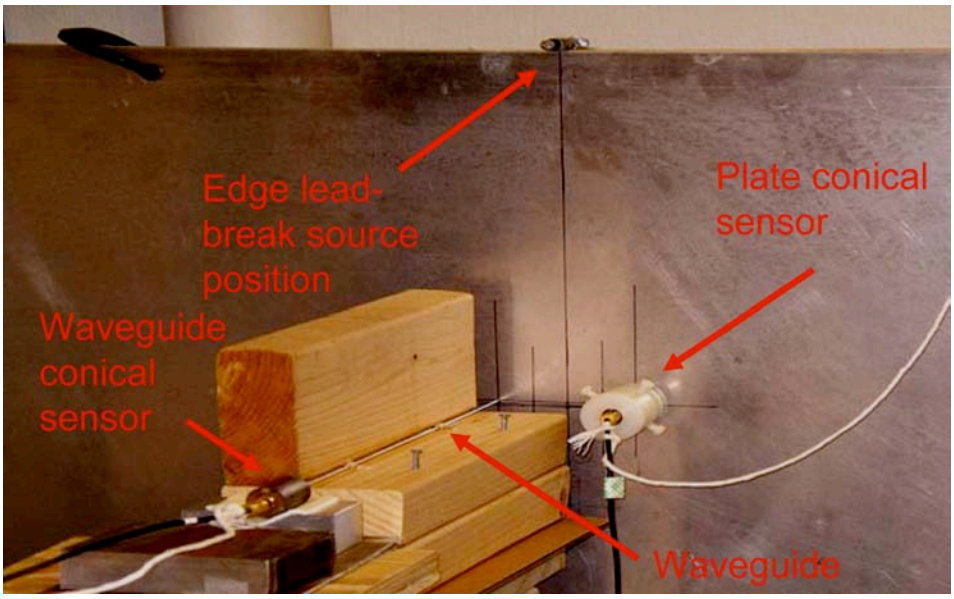


Fig. 3 Photograph of test setup for edge in-plane pencil-lead-break source.

The test setup is shown by photographs in Figs. 2 and 3. Pencil-lead breaks (0.3-mm diameter, 2H hardness and a length of about 2 mm) provided the source to generate the simulated AE signals. Both plate-top-surface out-of-plane (setup in Fig. 2) and plate-edge in-plane (setup in Fig. 3) pencil-lead breaks were applied on an aluminum alloy plate with a thickness of 3.1 mm. The transverse dimensions of the plate (1220 mm by 1525 mm) were large enough to preclude reflections from the plate edges arriving during the duration of the signals propagating directly from the pencil-lead break position to the plate-mounted sensor and the waveguide contact area. The waveguide (WG) as shown (see Figs. 2 and 3) was mounted perpendicular to the plate surface. The philosophy of the experimental approach was to have both the plate-mounted sensor and the WG contact area (with the plate) at 254 mm from the pencil-lead break point. Thus the differences in the signals from the two sensors can be attributed to the waveguide. This distance was sufficient to allow full development of Lamb waves.

Two WG materials were used: aluminum alloy rods with a diameter of either 1.59 mm or 3.18 mm, and brass rods with a diameter of 1.59 mm. No details on the exact alloys and their history were available. Prior to their use in the experiment, the ends of the rods were milled to provide a relatively smooth surface that was perpendicular to the axial direction of the rods. The nominal length of the WGs was 305 mm. Vacuum grease was used as a couplant for the two sensors and the WG-to-plate interface. In this initial study with wideband sensors and small diameter waveguides, no attempt was made to deal with the issues of coupling at other than room temperature. The two sensors and the WG were spring loaded (see the insert in Fig. 2) against their contact surfaces with a force of about 5 N.

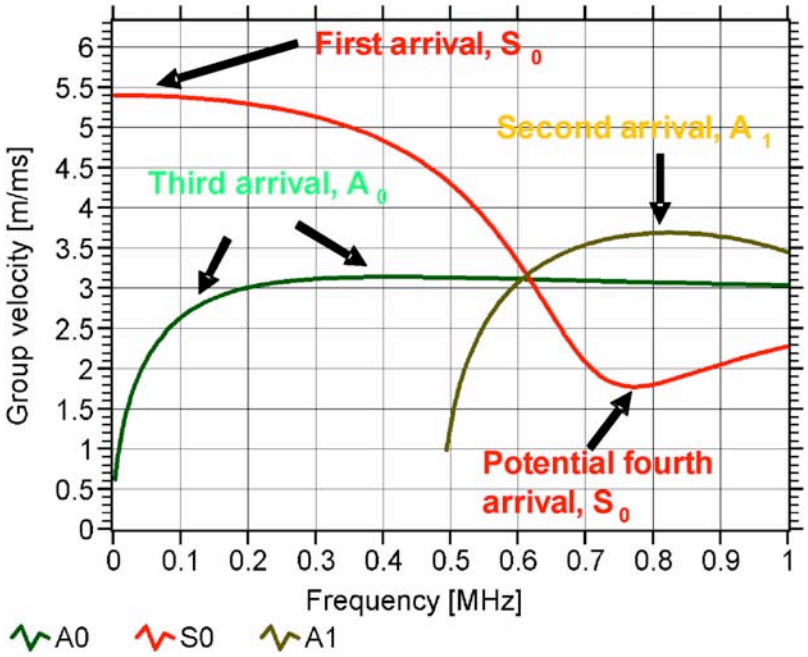


Fig. 4 Group velocity versus frequency for 3.1-mm thick aluminum plate showing $A_0$, $A_1$ and $S_0$ modes.

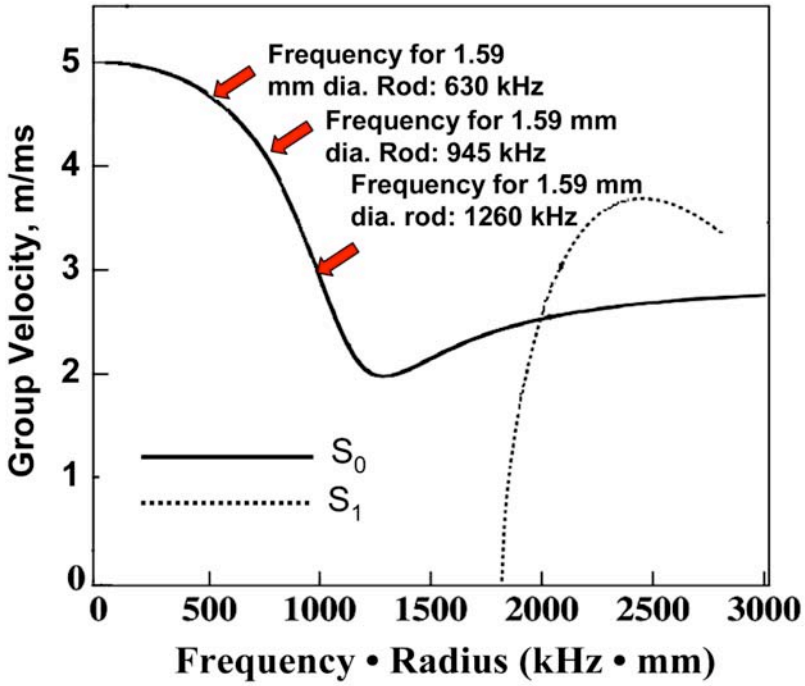


Fig. 5 Group velocity versus frequency•radius for aluminum rod showing $S_0$ and $S_1$ longitudinal modes (Adapted from Ono and Cho [1]).

**Discussion of Expected Waves in the Plate and Waveguides**

Due to the relatively small thickness of the plate, only lower Lamb modes were expected to be generated in the plate over the frequency range of interest. Figure 4 shows a plot of group velocity versus frequency of the lowest symmetric mode ($S_0$) and the two lowest anti-symmetric modes ($A_0$ and $A_1$) for the 3.1-mm thick plate. These curves were calculated (software reference

[5]) using Kolsky's [6] bulk velocities for aluminum. The frequency range in Fig. 4 was terminated at 1 MHz to correspond to the frequency range in Fig. 1.

Based upon the regions of the curves that are nearly stationary, as pointed out by Weaver and Pao [7], and the author's experience, the potential distinguishable sequence of arrivals in the pencil-lead-break-generated waves is pointed out in Fig. 4. Since the WG was oriented perpendicular to the plate surface and coupled by a viscous couplant, it was expected that the plate-end of the WG is significantly excited only by the out-of-plane displacement of the plate surface. Thus, only longitudinal waves were expected to be generated in the WGs. Figure 5 shows the group velocity versus frequency·radius of the two lowest longitudinal modes for the aluminum WGs. This figure was obtained by modifying a figure published by Ono and Cho [1].

For the signal from the WG-mounted sensor to closely duplicate the signal from the plate-mounted sensor, we assume that the input displacements from the plate to the end of the WG must be transmitted at the rod velocity (i.e., the velocity of the rod $S_0$ mode at near zero frequency). Such a transmission would mean the out-of-plane displacements from the sensor end of the rod into the WG-mounted sensor would be the same as if that sensor were mounted directly on the plate. Based on the $S_0$ group velocity curve shown in Fig. 5, this ideal situation would occur only for relatively low frequencies. But since the initial portion of the $S_0$ curve is relatively flat as the frequency • radius increases from zero for this range of frequencies in a small diameter WG, all these frequencies would be transmitted at about the same velocity. Thus, potentially the out-of-plane plate surface displacement might be preserved in the WG-mounted sensor signal.

To provide some perspective of how much the longitudinal-mode velocity might vary, the points that show the velocity at certain frequencies are shown in Fig. 5 for a 1.59-mm aluminum rod. Clearly up to about 630 kHz, the velocity is relatively constant, and the displacement as a function of frequency might be nearly preserved. Further, from examining Fig. 4 (plate group-velocity curves), we might expect that the first and third arrival regions would potentially be preserved. Contributing to this "preservation" would be the use of WGs that are not too long, since a very long WG would cause small velocity differences (for different frequencies) in the rod to produce significant propagation time differences. With WGs of larger diameter, the highest frequency that could be expected to travel at a velocity that would mostly preserve the signal would be lower.

**Experimental Results and Discussion**

An example of a typical set of experimental waveforms is shown in Fig. 6. In this case, the source was an out-of-plane pencil-lead break. A pre-trigger (based on the signal from the conical sensor mounted on the plate) was used to simultaneously trigger both recorder channels. The delay shown in the arrival of the signal from the 1.59-mm diameter aluminum WG sensor (Fig. 6(b)) was due to the propagation time along the length of the WG. In Fig. 6(b), the arrivals of the initial portion of the plate $S_o$ and $A_o$ modes are indicated for the WG-mounted sensor signal. These two arrivals are also obvious (see Fig. 6(a)) in the signal from the conical sensor coupled to the plate. In addition, based on the exact WG length (306.4 mm) and the aluminum rod velocity (5.09 mm/μs, [6]), an initial reflection in the WG of the plate $A_0$ mode was identified. This reflection is also indicated in Fig. 6(b). This reflection occurs after the signal in the WG has traversed its length three times after initially entering it. Due to its small amplitude, the plate $S_0$ mode reflection is not readily identified in this case.

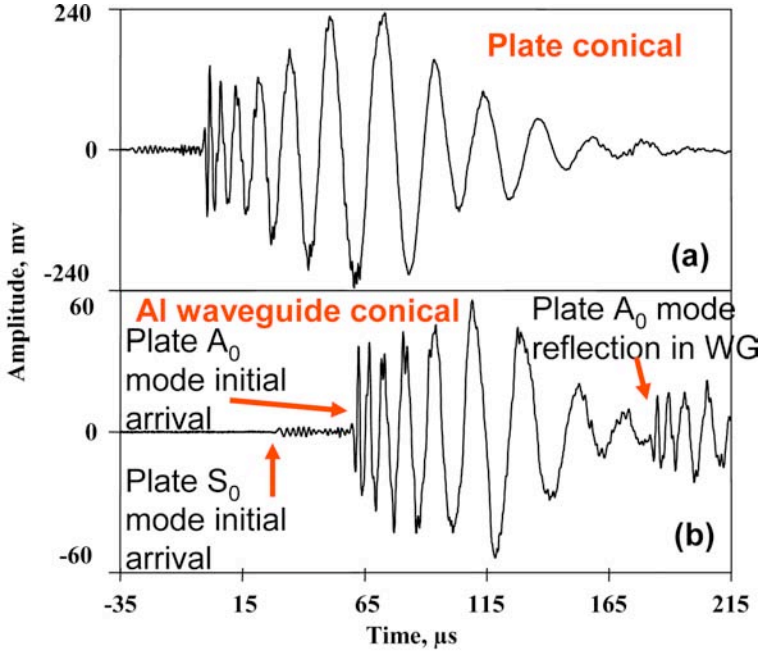


Fig. 6 Waveforms of signals from out-of-plane source with a 1.59-mm diameter by 306.4-mm long aluminum waveguide. Part (a) from plate conical sensor and part (b) from a conical sensor coupled to the end of the waveguide.

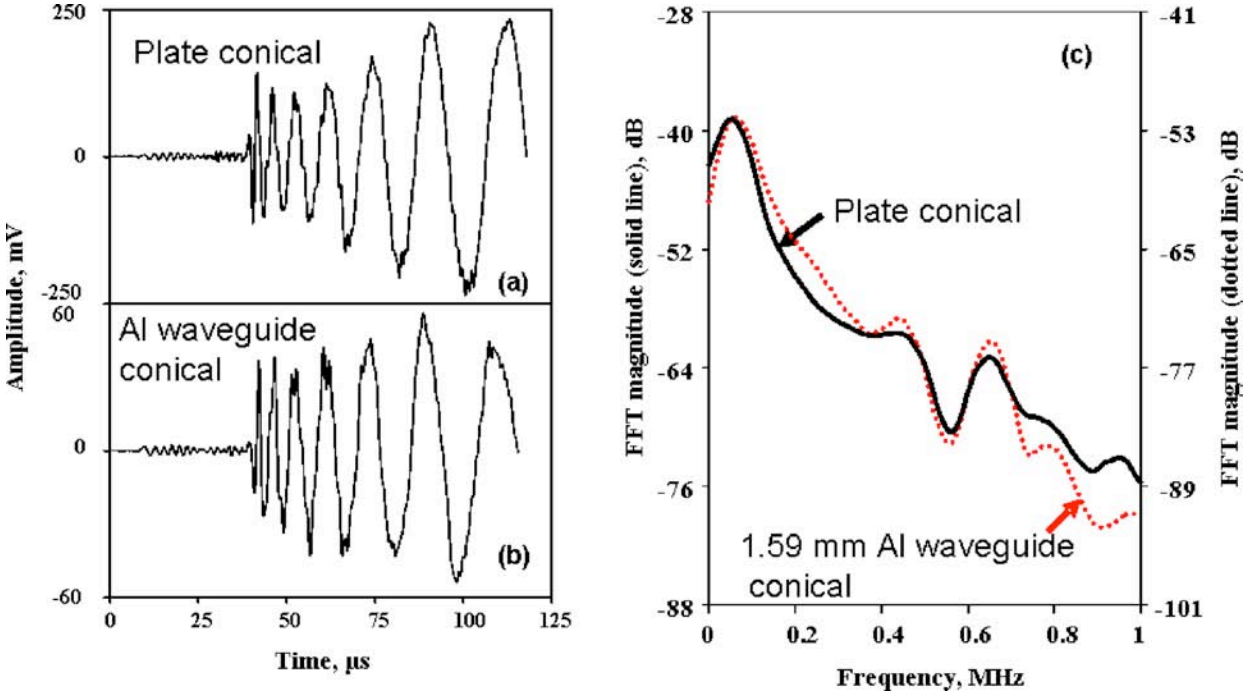


Fig. 7 Parts (a) and (b) are the same as those in Fig. 6, except that the offset in the waveguide sensor signal has been removed using the rod velocity and rod length. Also, the signals have been terminated at a zero prior to the reflection in the rod of the plate $S_0$ mode. Part (c) provides the FFT spectra of the two signals shown in parts (a) and (b).

Based upon the rod velocity and the WG length, the WG signal was offset forward by 60.2 µs to allow easier comparison of the signals from the two sensors. Figure 7 shows these signals from the plate and WG conical sensors terminated at a convenient zero prior to the expected reflection of the plate $S_0$ mode in the WG. The signals were terminated at zeros in preparation for

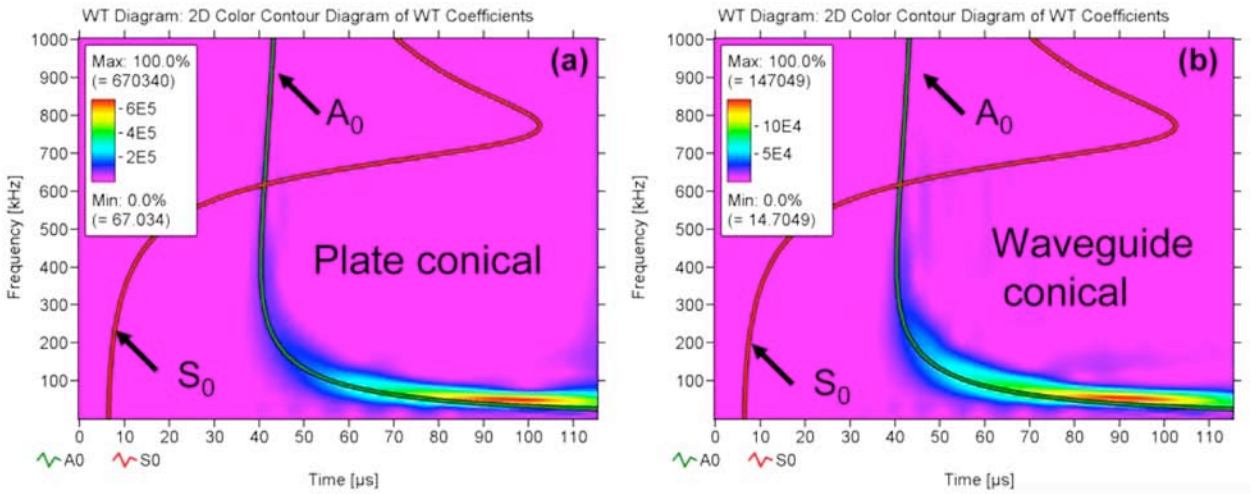


Fig. 8 WTs of the signals shown in Figs. 7(a) and (b) with the superimposed frequency versus propagation time (for 254-mm propagation distance) curves (based on group velocity curves) for the two lowest plate modes.

the calculation of the fast Fourier transform (FFT). The FFTs are shown in Fig. 7(c) over a frequency range from 0 to 1 MHz. The FFTs were calculated with a square window with the signals extended by zeros to a total length of 2048 points. For clarity, the resulting FFTs were smoothed over 30 points.

Examination of Fig. 7 shows that the signals from the plate and WG conical sensor are qualitatively very similar in both the time and frequency domains. In Fig. 7(c), the amplitude scales of the FFT results were adjusted to superimpose the results from zero to about 100 kHz (this procedure was used for all such FFT comparisons in this paper). As expected, the WG signal was reduced in amplitude. The reduction is about 13 dB, based on the offset of the magnitude scales to superimpose the FFT results.

At frequencies above about 700 kHz, the WG signal experienced a further reduction in the response level compared to the plate sensor response. The wavelet transforms (WTs) [8] of the two signals in Figs. 7(a) and (b) were calculated, and they are shown in Fig. 8 with superimposed $S_0$ and $A_0$ plate modes. These modes were superimposed by visually adjusting their time offset after the 254-mm propagation distance had been accounted for in the calculation of the propagation time. The key parameters chosen for the WT calculation were a frequency resolution of 3 kHz and a wavelet size of 600 samples. Clearly, the WT results also demonstrate the strong similarity of the signal from the WG sensor to that from the plate sensor.

In order to compare the WG sensor signal with the plate sensor signal when the signal in the plate was not as strongly dominated by the flexural, $A_0$, mode, an edge pencil-lead break was used. For this case, the configuration already shown in Fig. 3 was used with the contact point of the pencil lead being near the mid-plane of the edge of the plate. Figure 9 shows the two simultaneously recorded signals when the 1.59-mm diameter aluminum WG was used. As before, the initial regions of the $S_0$ and $A_0$ modes are indicated in Fig. 9. In addition, the plate $S_0$-mode reflection in the WG signal is pointed out in Fig. 9(b). As before, this reflection arrival was identified based on the calculated propagation time at the aluminum rod velocity for two additional WG lengths after its original arrival at the WG sensor.

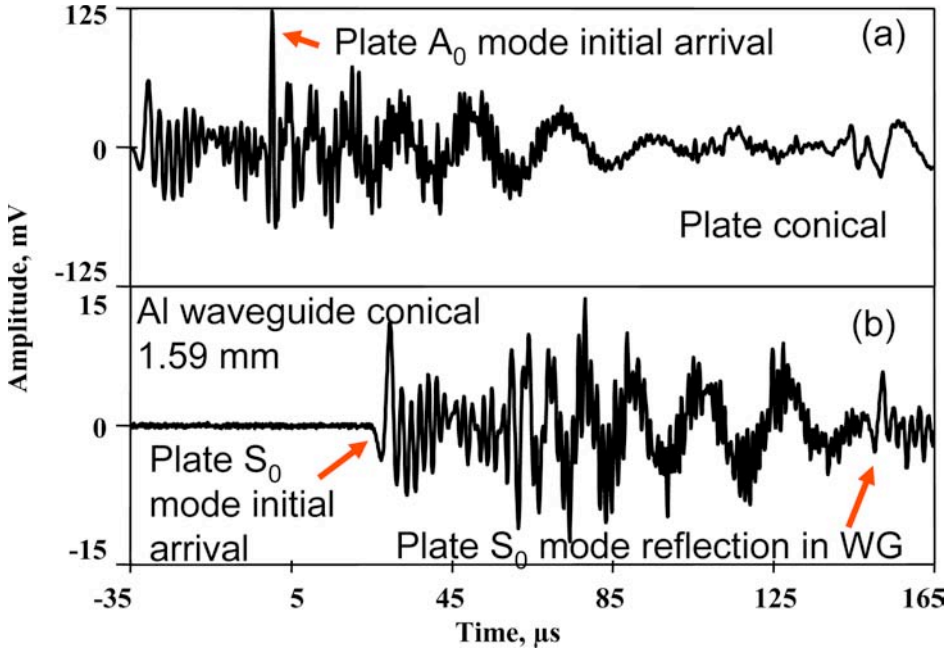


Fig. 9 Waveforms of signals from an edge, near-midplane pencil-lead break source with a 1.59 mm diameter by 306.4 mm long aluminum waveguide. Part (a) from the plate conical sensor and part (b) from the conical sensor coupled to the end of the waveguide.

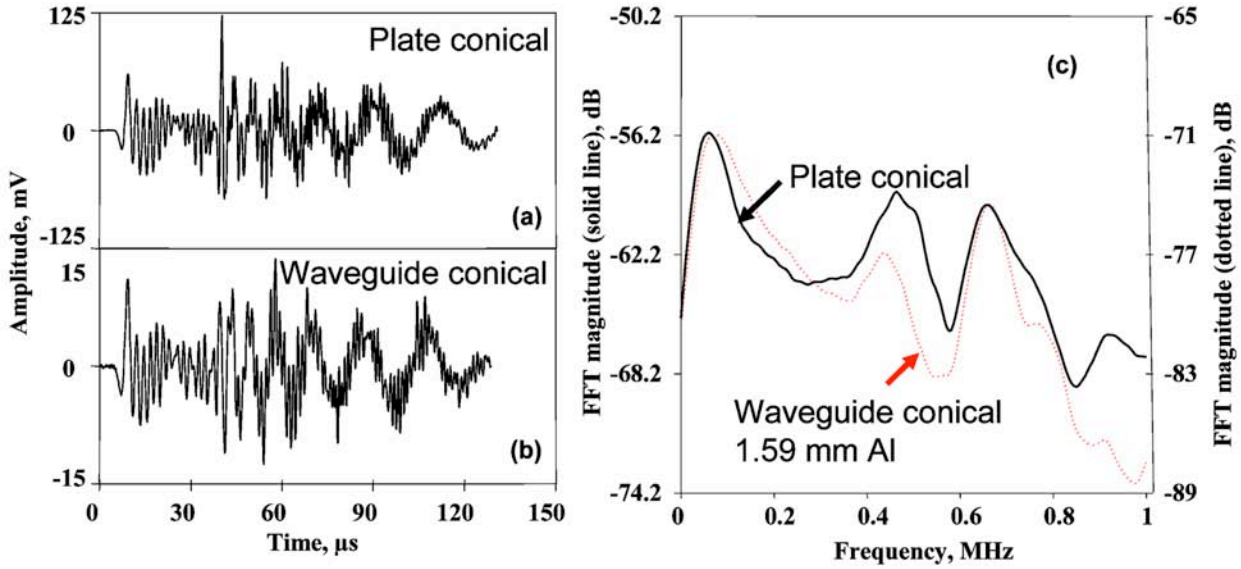


Fig. 10 Parts (a) and (b) are the same as those in Fig. 9, except for the conditions described in the caption of Fig. 7. Part (c) shows the FFT spectra of the two signals shown in parts (a) and (b).

To continue the comparison, the WG signal was offset as before by the rod-length transit time at the rod velocity. Figures 10(a) and (b) show both signals with a termination at a convenient zero before the plate $S_0$-mode reflection in the rod. In the same way as described earlier, the FFTs and the WTs were calculated, and the results are displayed in Figs. 10(c) and 11, respectively. In this case the amplitude of the WG sensor signal is down about 17 dB from the plate sensor signal as can be seen from the offset used in the FFT results. It should be noted that these comparisons should be viewed as a general trend since the "convenient" zero does not lead to the same signal length for the various cases in this paper and the variations in signal length occur in the region of the signal dominated by lower frequencies. Again the out-of-plane displacement

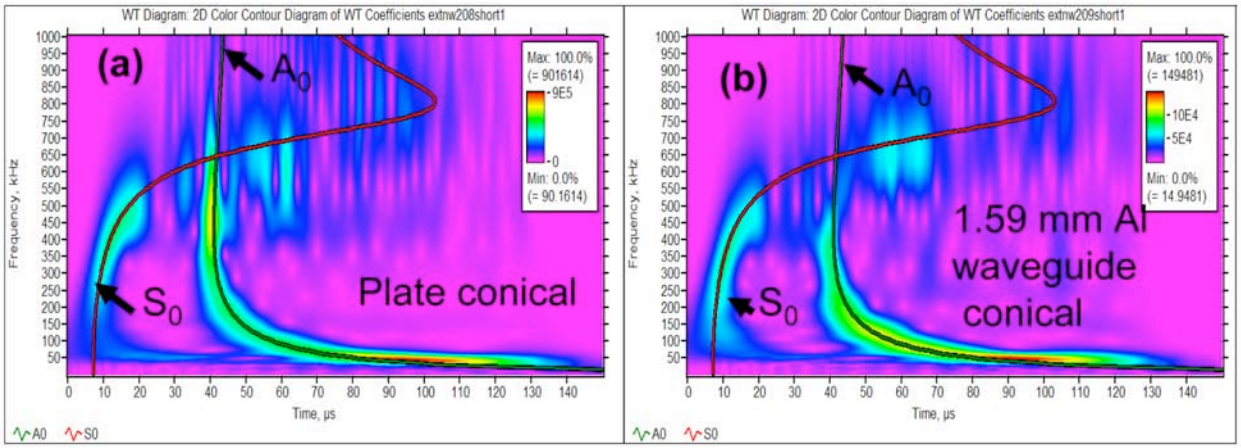


Fig. 11 WTs of the two signals shown in Figs. 10(a) and (b) with superimposed results from the $A_0$ and $S_0$ plate modes for a 254-mm propagation distance in the plate.

signals, FFTs and WTs are qualitatively quite similar. There is again a further reduction in the WG sensor signal at higher frequencies when compared to the plate sensor. This reduction is somewhat more than that seen with the out-of-plane pencil-lead break case (compare Figs. 7(c) and 10(c)). There is also some deviation between 400 kHz to 600 kHz in these FFT results.

It is possible that a part of the deviation of the WG sensor signal compared to the plate sensor signal is due to the fact that the edge of the aluminum plate had been sheared rather than machined. This may have resulted in a slightly different signal arriving at the plate sensor compared to that arriving at the point where the WG was coupled to the plate. It should also be noted that the WTs of both signals clearly show that both the $A_0$ and $S_0$ modes are present in both the plate and WG sensor signals. As described before, the plate group velocity curves for the $A_0$ and $S_0$ modes were superimposed on the WT results visually.

**Larger Diameter Aluminum WG**

Based on Fig. 5 and the accompanying discussion, a larger diameter WG was expected to result in a poorer duplication by the WG sensor signal of the signal from a plate-mounted sensor. Nevertheless a 3.18-mm diameter aluminum WG was tested with an out-of-plane pencil-lead break source on the plate. The results are shown in Figs. 12 and 13. Figures 12(a) and (b) demonstrate that the displacement signals from both sensors (after the WG sensor signal had been shifted forward by 80.5 µs, based on its exact rod length of 409.6 mm and the rod velocity) terminated at a zero before the plate $A_0$ mode reflection. The overall view seems to lead to the conclusion that the WG sensor signal is quite similar to the plate sensor signal, but a later closer examination will show some distinct differences.

The FFT and WT results in Figs. 12(c) and 13 respectively show fairly similar results between the signals from the two sensors. Based on the FFTs for this larger diameter case, the additional reduction of the WG sensor signal compared to the plate sensor signal begins at a lower frequency of about 300 kHz compared to that seen in the case of the 1.59 mm WG. In contrast to the smaller diameter WG, the signal amplitude decrease of about 5 dB with the 3.18 mm WG (based on the FFT offset used) was considerably less than the decrease of about 13 dB with the 1.59 mm diameter WG. For the same reasons noted before, these amplitude differences should be viewed as a trend indicator.

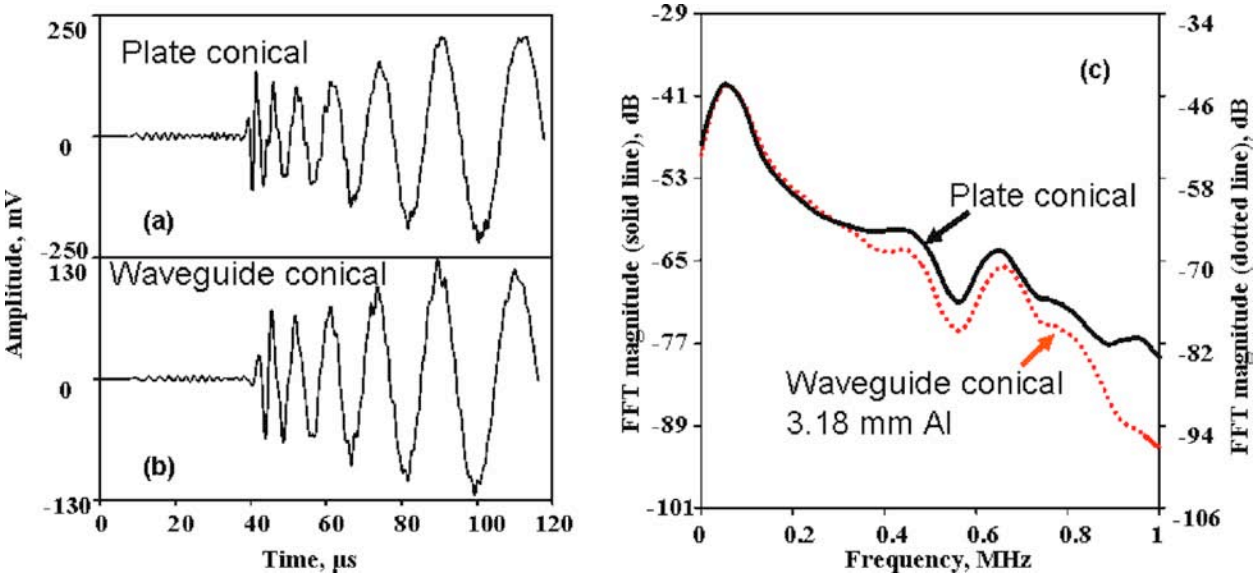


Fig. 12 Waveforms of signals from an out-of-plane pencil-lead break source with a 3.18-mm diameter aluminum waveguide of 409.6 mm length. Results are shown after the process described in the caption of Fig. 7. Part (c) provides the FFT spectra of the two signals shown in parts (a) and (b).

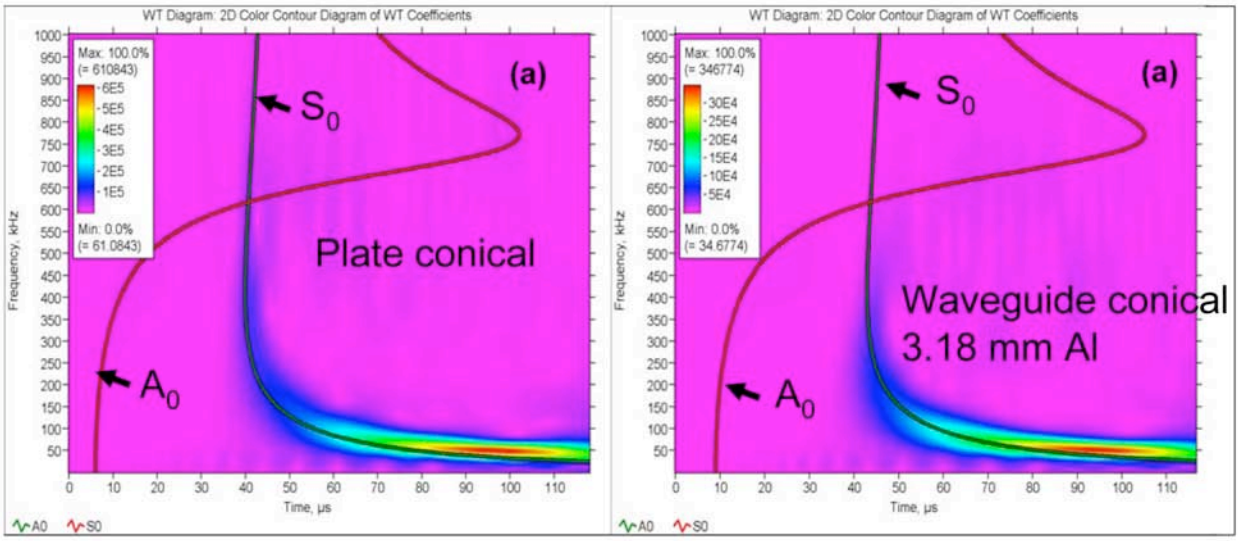


Fig. 13 WTs of the two signals shown in parts (a) and (b) of Fig. 12 with superimposed result from the two lowest plate group-velocity modes.

To examine more closely differences between the two diameters of the aluminum WGs, the signals were compared more directly in Figs. 14(a) and (b). In these figures, the time scale was changed so that the initial portion of the $S_0$ mode and the first few cycles of the plate flexural $A_0$ mode are shown, and the amplitude scales for the two curves were adjusted to enhance the comparisons. These results show (comparing Figs. 14(a) and (b)) for the larger diameter WG that there is a loss of duplication in the WG sensor signal of the $S_0$ mode just a few cycles after it arrives, and there is a more serious loss of duplication in the first two cycles of the arrival of the $A_0$ mode.

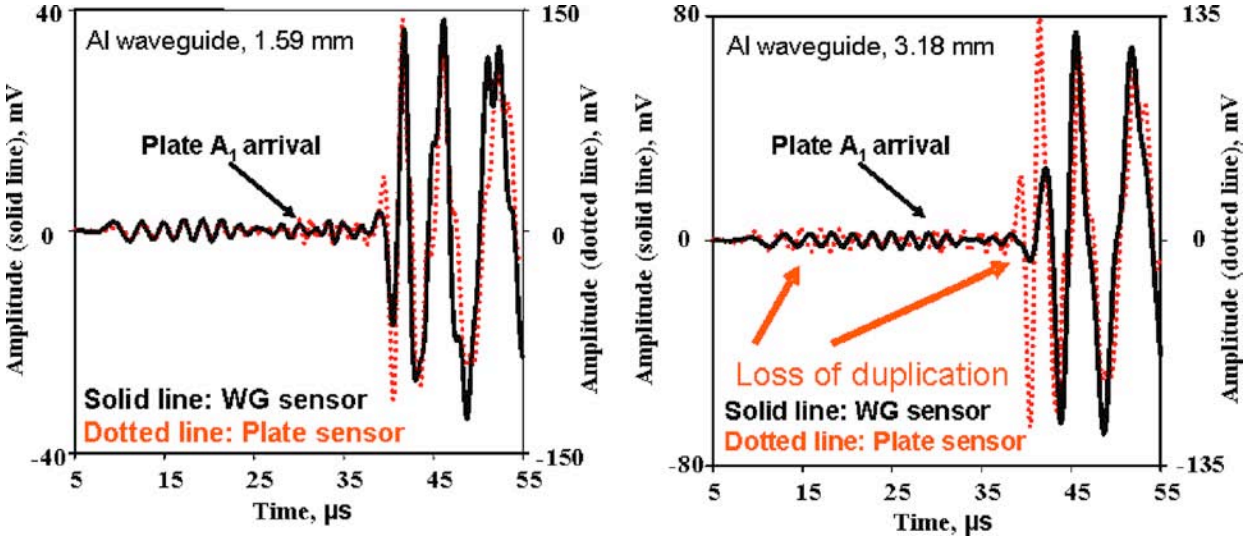


Fig. 14 Initial portions of the two sensor signals (after removal of the off-set due to the propagation time at the rod velocity) for the two aluminum waveguide cases with an out-of-plane pencil-lead break. Part (a) for the 1.59-mm diameter waveguide and part (b) for the 3.18-mm diameter waveguide.

It is relevant to point out that this latter deviation is in the high frequency region of that plate mode. It is not surprising that the duplication results are better for the smaller diameter WG (see Fig. 14(a)), where a larger portion of the frequencies of interest travel at or near the rod velocity. In the case of the larger diameter WG, the higher frequencies of the plate $S_0$ and $A_0$ modes that are transferred to the WG travel over a wider range of velocities in the rod $S_0$ mode, and thus those parts of the plate signal are dispersed and have less amplitude in the WG sensor signal. It is also relevant to point out that the larger diameter WG is longer, so small variations in the velocities in the rod would have a larger effect.

As a final observation from Fig. 14, the arrival of the beginning of the plate $A_1$ mode is indicated in the plate sensor signal. Since the plate group velocity diagram (shown in Fig. 4) indicates that the $A_1$ mode arrives with frequencies from about 800 kHz to 1000 kHz, it is not surprising that it is difficult to detect this arrival in the WG sensor signal in either diameter case.

**Small Diameter Brass WG**

To examine a case where the acoustic impedance of the WG does not match that of the plate, a small diameter (1.59 mm) brass rod was used with an out-of-plane pencil-lead break. As before, the simultaneously gathered signals were offset in time due to the added propagation time along the WG length of 300.4 mm. Since the exact rod velocity was unknown, the value (3.67 mm/µs) given by Kolsky [6] for copper was used with the rod length to correct for the offset in time between the two signals. Figures 15(a) and (b) show the resulting signals. In this figure both sensor signals were terminated at a zero prior to the plate $A_o$ mode reflection in the brass WG. Figure 15(c) shows the FFT of the two time-domain signals. As before, the FFTs were calculated with a square window after they were extended to 2048 points from their zero-terminated length.

Qualitatively, in Figs. 15(a) and (b), the time domain signals are quite similar. The FFT result (after again changing the vertical scale to superimpose the results in the low frequency

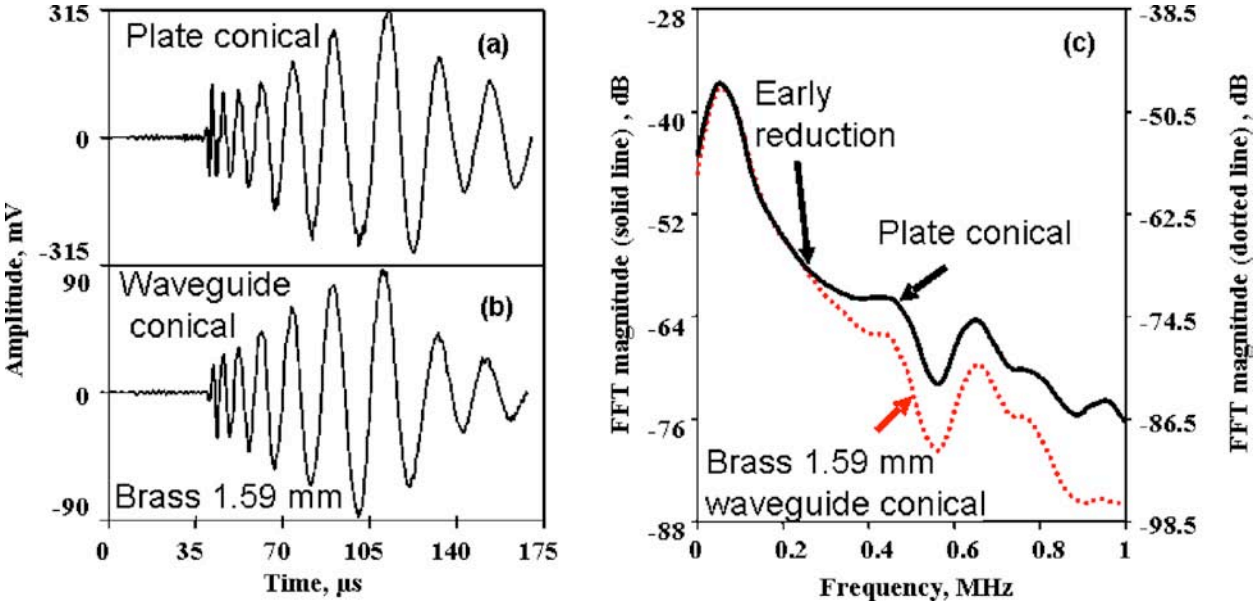


Fig. 15 Waveforms of signals from an out-of-plane pencil-lead break source with a 1.59 mm diameter by 300.4 mm long brass waveguide. Part (a) from the plate conical sensor signal and part (b) from the sensor coupled to the end of the brass waveguide. Signals are shown after the removal of the time offset as described in the caption of Fig. 7. Part (c) shows the FFT spectra of the signals shown in parts (a) and (b).

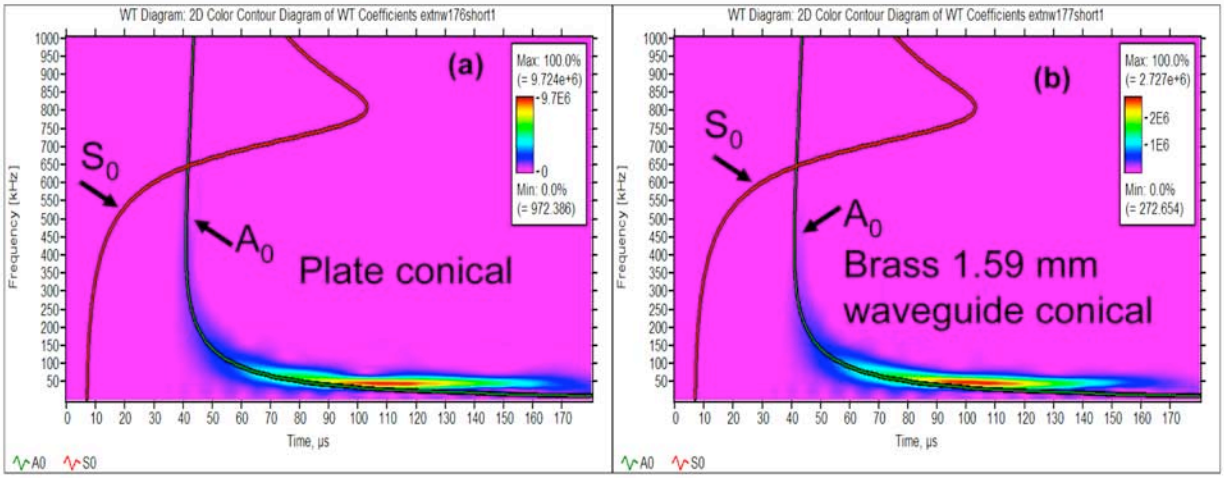


Fig. 16 WTs of the two signals shown in parts (a) and (b) of Fig. 15 with superimposed results from the two lowest plate modes group-velocity curves.

region) shows that the WG sensor signal starts to fall off at about 300 kHz relative to the plate sensor signal. As before, to help clarify the FFT results, the curves were smoothed over 30 points. With the limitations already pointed out, the FFT results indicate an amplitude decrease of about 11 dB of the WG sensor signal as compared to the plate sensor signal. This result compares with the approximately 13-dB loss for the same source with the aluminum rod WG (see Fig. 7(c)). As shown in Fig. 16, the WT results (calculated as described earlier) are very similar for the plate and WG sensors, and this figure shows the dominance of the low-frequency portion of the $A_0$ mode.

To show more closely the differences between the WGs of the two different materials of the same diameter (1.59 mm), the initial arrivals of the signals through the first few cycles of the $A_0$

mode are compared in parts (a) and (b) of Fig. 17. For the aluminum and brass WGs, each part of the figure shows the WG sensor signal stacked (by adjusting the vertical scales) with the plate sensor signal. The arrows in part (b) show the regions of poor duplication of the brass WG sensor signal compared to the plate sensor signal. Part (a) clearly shows that in these regions the duplication of the aluminum WG signal is much closer to that of the plate sensor signal.

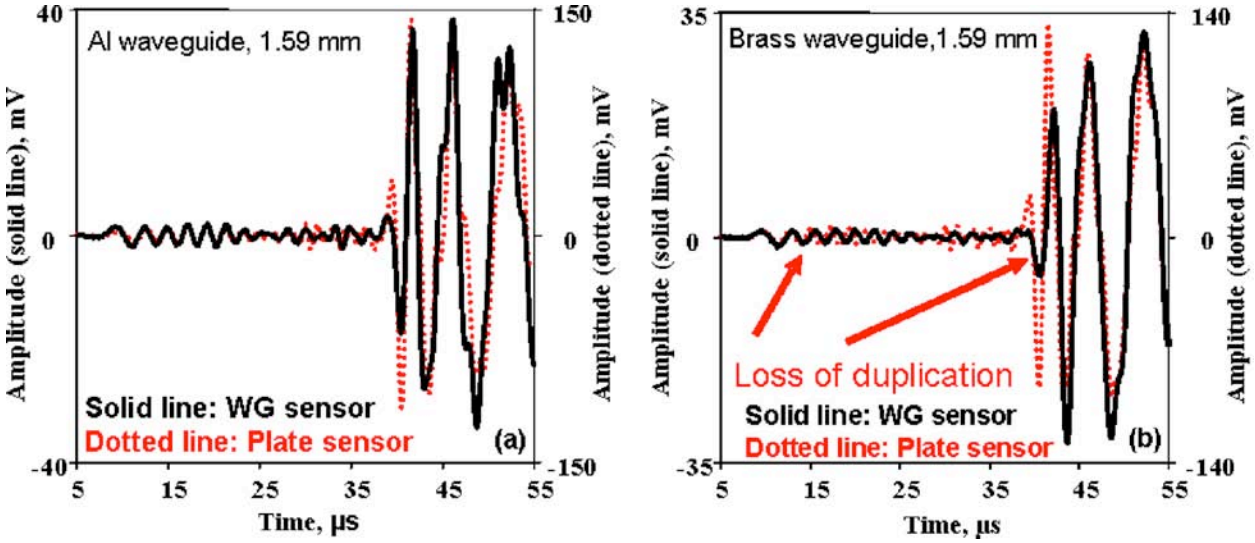


Fig. 17 Initial portions of the plate and waveguide sensor signals after the offset in time has been removed for the out-of-plane pencil-lead-break source and a waveguide diameter of 1.59 mm. Part (a) is for the aluminum waveguide and part (b) is for the brass waveguide.

## Conclusions

The experiments presented here demonstrated that when a small 1.59-mm diameter waveguide was used with a wideband conical, nearly-flat-with-frequency sensor, the waveguide sensor can provide a wideband high-fidelity signal over the range of frequencies and Lamb modes generated by pencil-lead breaks in a thin aluminum plate. Specifically, one can conclude:

- A 1.59-mm diameter aluminum WG transmits a reasonable copy of the out-of-plane displacement that passes under the end of the waveguide coupled to the plate.
- The 1.59-mm diameter aluminum waveguide provides a better duplicate of the plate sensor signal than a 3.18-mm diameter rod of the same material.
- The superiority of the 1.59-mm diameter aluminum rod waveguide is particularly apparent at the beginning of the signal from the plate $A_0$ mode and part way through the initial portion of the signal from the plate $S_0$ mode.
- The signal regions where the larger diameter aluminum rod waveguide sensor does the poorest job of duplicating the plate sensor signal are those where higher frequencies are present. These frequency regions of the rod $S_0$ mode are those where the displacement waves are traveling at slower velocities than the rod velocity.
- The experimental results with the 1.59-mm brass rod mirror those of the 3.18-mm aluminum rod in the degradation of certain frequency regions in the waveguide sensor signal.
- In all cases, the signal level out of the waveguide end-mounted sensor is reduced in comparison to that for the plate-mounted sensor.

- The WG signal reduction trends in signal level for the out-of-plane pencil-lead break source are about 13 dB for the 1.59-mm aluminum waveguide, 5 dB for the 3.18-mm aluminum waveguide, and 11 dB for the 1.59-mm brass waveguide.

**Acknowledgement**

The efforts of Mr. David McColskey and Mr. Raymond Santoyo of NIST Boulder, Colorado in assisting with the experimental setup are acknowledged.

**References**

1. K. Ono, and H. Cho, "Rods and Tubes as AE Waveguides", J. of Acoustic Emission, **22**, 243-252 (2004). See also *Proceedings 26th European Conference on Acoustic Emission Testing*, Vol. 2, pp. 593-597, 2004.
2. M.A. Hamstad and C.M. Fortunko, "Development of Practical Wideband High Fidelity Acoustic Emission Sensors", *Nondestructive Evaluation of Aging Bridges and Highways*, Steve Chase, Editor, Proc. SPIE 2456, pp. 281-288, 1995.
3. M.A. Hamstad, "Improved Signal-to-Noise Wideband Acoustic/Ultrasonic Contact Displacement Sensors for Wood and Polymers", Wood and Fiber Science, **29** (3), 239-248, 1997.
4. Fuji Ceramics Corporation, Japan, Model A1002.
5. J. Vallen, "Vallen Dispersion Software, Version R2005.1121", Vallen-Systeme GmbH, Munich, Germany. Available as http://www.valleh.de/wavelet/index.html, 2005.
6. H. Kolsky, *Stress Waves in Solids*, Dover Publications Inc., New York, 1953.
7. R. L. Weaver and Y.-H. Pao, "Axisymmetric Elastic Waves Excited by a Point Source in a Plate," J. of Appl. Mech., Col. **49**, 821-836, 1982.
8. J. Vallen, "AGU-Vallen Wavelet Transform Software, Version R2005.1121", Vallen-Systeme GmbH, Munich, Germany. Available at http://www.vallen.de/wavelet/index.html, 2005.